Observability Analysis of Opportunistic Receiver Localization with LEO Satellite Pseudorange Measurements

Ralph Sabbagh, *University of California, Irvine*

Zaher M. Kassas, *The Ohio State University*

BIOGRAPHY

Ralph Sabbagh is a Ph.D. student in the Department of Mechanical and Aerospace Engineering at the University of California, Irvine and a member of the Autonomous Systems Perception, Intelligence, and Navigation (ASPIN) Laboratory. He received a B.E. in Mechanical Engineering with High Distinction from the American University of Beirut. His research interests include satellite-based opportunistic navigation and estimation theory.

Zaher (Zak) M. Kassas is a Professor at The Ohio State University and director of the Autonomous Systems Perception, Intelligence, and Navigation (ASPIN) Laboratory. He is also director of the U.S. Department of Transportation Center: CARMEN (Center for Automated Vehicle Research with Multimodal AssurEd Navigation), focusing on navigation resiliency and security of highly automated transportation systems. He received a B.E. in Electrical Engineering from the Lebanese American University, an M.S. in Electrical and Computer Engineering from The Ohio State University, and an M.S.E. in Aerospace Engineering and a Ph.D. in Electrical and Computer Engineering from The University of Texas at Austin. He is a recipient of the 2018 National Science Foundation (NSF) CAREER award, 2019 Office of Naval Research (ONR) Young Investigator Program (YIP) award, 2022 Air Force Office of Scientific Research (AFOSR) YIP award, 2018 IEEE Walter Fried Award, 2018 Institute of Navigation (ION) Samuel Burka Award, and 2019 ION Col. Thomas Thurlow Award. He is a Senior Editor of the IEEE Transactions on Intelligent Vehicles and an Associate Editor of the IEEE Transactions on Aerospace and Electronic Systems and the IEEE Transactions on Intelligent Transportation Systems. His research interests include cyber-physical systems, navigation systems, autonomous vehicles, and intelligent transportation systems.

ABSTRACT

An observability analysis of terrestrial receiver localization via pseudorange measurements extracted from a single low Earth orbit (LEO) satellite is presented. It is concluded that a stationary receiver with an unknown state (position and time) can localize itself with measurements from a LEO satellite with a known state (position, velocity, and time). In addition, bounds on the determinant of the observability matrix are derived. The relationship between the satellite's relative orbital inclination angle and geometric diversity of the line-of-sight vectors from the receiver to the satellite is analyzed, leading to geometric interpretations indicating directions of poor observability. Experimental results are presented showcasing the conclusions of the observability analysis for a receiver localizing itself with a single Starlink LEO satellite or a single Orbcomm LEO satellite. Finally, an observability-aided LEO satellite selection strategy is discussed.

I. INTRODUCTION

We are witnessing the era of Low Earth orbit (LEO) satellite megaconstellations (Reid et al., 2020; Kulu, 2021). These megaconstellations promise to revolutionize several domains, bringing unprecedented high-resolution images; remote sensing; and global, high-availability, high-bandwidth, and low-latency Internet (Liu et al., 2021; Judice et al., 2022; Okasha et al., 2022). Due to LEO satellites' inherently desirable attributes (Kassas et al., 2019), namely: (i) geometric and spectral diversity, (ii) abundance, (iii) high received signal power, and (iv) high orbital velocity, LEO satellites offer an attractive alternative to global navigation satellite systems (GNSS), which reside in medium Earth orbit (MEO) (Reid et al., 2021; Kassas, 2021; Prol et al., 2022; Jardak and Jault, 2022). The promise of utilizing LEO satellites for navigation has been the subject of numerous recent theoretical (Wei et al., 2020; Thompson et al., 2020; Psiaki, 2021; Nardin et al., 2021; Hartnett, 2022; Cassel et al., 2022; Jiang et al., 2022; Iannucci and Humphreys, 2022; Elgamoudi et al., 2020) and experimental (Tan et al., 2019; Farhangian and Landry, 2020; Farhangian et al., 2021; Wang and El-Mowafy, 2022; Huang et al., 2022; Li et al., 2022; Khalife et al., 2022; Neinavaie et al., 2022; Zhao et al., 2022) studies.

LEO satellites orbit the Earth at much higher rates than GNSS satellites. Contrast, for example, the orbital period of a GPS MEO satellite (11 hr, 58 min) with that of Orbcomm LEO satellites (about 99 min) and Starlink LEO satellites (about 96 min). This yields significant change in their geometry, which can be exploited to localize a terrestrial receiver with fewer satellites. In

particular, while four GNSS satellites are needed to estimate the states of the receiver via a static estimator (e.g., nonlinear least squares), a single LEO satellite can be used to localize the receiver via a dynamic estimator (e.g., an extended Kalman filter (EKF)) by fusing consecutive LEO measurements taken over a relatively short period of time. A few studies demonstrating the impact of receiver localization using a small number of satellites have been conducted in the literature. In (Pike et al., 2022), pseudorange and Doppler measurements were combined for stationary receiver positioning using two and three satellites without the use of a base station or differential positioning techniques.

Observability analysis with LEO satellites has been studied in the context of space situational awareness with relative position measurements (Ou and Zhang, 2018; Yong and Zhang, 2019; Friedman, 2020) and orbit determination with angles-only measurements (Kaufman et al., 2016; Sullivan et al., 2018; Friedman and Frueh, 2021). Moreover, observability of *planar* environments comprising terrestrial transmitters with unknown positions and time have been studied in (Kassas and Humphreys, 2012), where estimability was *numerically* assessed from the EKF's estimation error covariance, and in (Morales and Kassas, 2019), where the Riccati equation was analyzed to conclude that *simultaneously* estimating the receiver's and transmitter's time is stochastically unobservable. However, observability analysis with a small number of LEO satellites in the context of localization has not been thoroughly studied. In (Sabbagh and Kassas, 2023), an observability analysis of *three-dimensional* receiver localization via pseudorange measurements extracted from the signals of a single LEO satellite was conducted. It was shown that a stationary receiver with an unknown state (position and time) can theoretically localize itself with a LEO satellite with a known state (position, velocity, and time). In addition, *analytical* bounds on the determinant of the -step observability matrix were derived indicating directions of poor observability. It was concluded that the system becomes unobservable if the receiver is in the satellite's orbital plane or along the normal to the satellite's orbital plane.

This paper aims to summarize the results presented in (Sabbagh and Kassas, 2023), with an emphasis on the implications of the analysis on observability-aided LEO satellite selection. Namely, empirical surface plots of the observability matrix can aid in selecting the satellite with desired (i) visibility duration, (ii) elevation profile, and (iii) altitude and relative orbital inclination angle. Finally, experimental results are presented showcasing the conclusions of the observability analysis for a receiver localizing itself with a single Starlink satellite or a single Orbcomm satellite.

The remainder of the paper is organized as follows. Section II describes the dynamics and measurement models. Section III analyzes analytically the observability of receiver localization using pseudorange measurements from a single LEO satellite and gives geometric interpretations of the derived results. Section IV presents experimental results with Orbcomm and Starlink LEO satellites, demonstrating the implications of the observability analysis on the estimation performance. Section V presents a discussion on observability-aided LEO satellite selection for improved receiver localization.

II. PRELIMINARIES AND MODEL DESCRIPTION

1. *Observability of LTV Systems*

Consider the discrete-time (DT) linear time-varying (LTV) dynamical system Σ given by

$$\Sigma : \begin{cases} x(k+1) &= \quad (k)\,x(k) + \quad (k)\,u(k) \\ y(k) &= \quad (k)\,x(k) \end{cases} \tag{1}$$

where $x \in$, $u \in$, and $y \in$ are the system state, input, and measurement vectors at time-step k, respectively, and $k \in$. The state transition matrix corresponding to Σ from time-step to time-step is given by

$$\Phi(\quad) \triangleq \begin{cases} (\;-1)\;(\;-2)\cdots(\;) & \text{if} \\ \quad_\times & \text{if} \;= \end{cases}$$

where $_\times$ denotes an $\times$ identity matrix. The following theorem characterizes the observability of DT LTV systems via the -step observability matrix (Rugh, 1996).

Theorem I: The DT LTV system (1) is -step observable if and only if its corresponding -step observability matrix

$$\mathcal{O}(k, k+\;-1) \triangleq \begin{bmatrix} (k)\,\Phi(k, k) \\ (k+1)\,\Phi(k+1, k) \\ \vdots \\ (k+\;-1)\,\Phi(k+\;-1, k) \end{bmatrix} \tag{2}$$

is full rank. Theorem I can be applied to nonlinear systems by linearizing at each time-step $\mathbf{k}$ around $x(\mathbf{k})$. The achieved observability results therein will only be valid locally (Huang et al., 2010).

2. *Receiver Dynamics*

The terrestrial receiver's position $r \in \mathbb{R}^3$ is assumed to be fixed in the Earth-centered inertial (ECI) frame and its distance from the center of Earth is denoted by $= \|r\|_2$. The dynamics of the receiver's clock error states (i.e., bias δt and drift $\dot{\delta t}$) is modeled as a double integrator driven by process noise (Bar-Shalom et al., 2002). The receiver's dynamics is given by

$$x(\mathbf{k}+1) = \ x(\mathbf{k}) + w(\mathbf{k})$$

where $x \triangleq \left[r^{\mathsf{T}}, c\,\delta t, c\,\dot{\delta} \right]^{\mathsf{T}}$ is the receiver's state vector, denotes the speed of light, and w is a process noise modeled as a zero-mean white random sequence with covariance $= \mathrm{diag}\left[\ _{3\times3} \ \right]$. The receiver state matrix is

$$= \begin{bmatrix} \ _{3\times3} & \ _{3\times2} \\ \ _{2\times3} & \ _{\mathrm{clk}} \end{bmatrix} \qquad _{\mathrm{clk}} = \begin{bmatrix} 1 & \\ 0 & 1 \end{bmatrix}$$

where is the sampling period. In this letter, the simplest receiver dynamics was considered to focus on the change in geometry due to the moving satellite. More elaborate receiver dynamics could be considered in future work.

3. *LEO Satellite Dynamics*

The LEO satellite is assumed to follow a circular Keplerian orbit with fixed inclination and a prescribed orbital radius denoted by $= \|r( )\|_2$ where 0 . Under the action of Earth's gravitational field, the satellite's orbital dynamics in continuous-time will be assumed to follow a simplified two-body model given by

$$\ddot{r}( ) = -\frac{\mu}{\ ^3}\,r( ) + w( ) \tag{3}$$

where $r \in \mathbb{R}^3$ is the satellite's position in the ECI frame and w is a process noise vector of acceleration perturbations resulting from Earth's non-uniform gravitational potential, atmospheric drag, solar radiation pressure, gravitational pull of other celestial bodies, and general relativity (Montenbruck and Gill, 2000). The following constraints on the satellite dynamics hold $\forall$ 0

$$\langle r( )\ r( )\rangle = \ ^2$$
$$\langle r_s( )\ r_s( )\rangle = \alpha^2 \ ^2$$
$$\langle r( )\ r_s( )\rangle = 0$$

where $\alpha^2 \triangleq \mu/a^3$. The dynamics of the satellite's clock bias δt and drift $\dot{\delta t}$ are modeled similarly to the receiver's clock error dynamics (Bar-Shalom et al., 2002). Next, the satellite dynamics in (3) can be discretized at a sampling period to yield

$$x(\ _{+1}) = \ x( ) + w( )$$

where $x = \left[r^{\mathsf{T}}\ \dot{r}^{\mathsf{T}}, c\,\delta t, c\,\dot{\delta} \right]^{\mathsf{T}}$ is the satellite's state vector and w is a process noise modeled as a zero-mean white random sequence with covariance , and is given by

$$= \begin{bmatrix} \cos(\alpha T)\ _{3\times3} & (1/\alpha)\sin(\alpha T)\ _{3\times3} & \ _{3\times2} \\ -\alpha\sin(\alpha T)\ _{3\times3} & \cos(\alpha T)\ _{3\times3} & \ _{3\times2} \\ \ _{2\times3} & \ _{2\times3} & \ _{\mathrm{clk}} \end{bmatrix}$$

4. *Measurement Model*

The pseudorange measurement extracted by the receiver (Pinell, 2021) from the satellite signals at time-step $\mathbf{k}$, after compensating for ionospheric and tropospheric delays (Kassas, 2021), is modeled as

$$\rho(\mathbf{k}) = \|r - r(\mathbf{k})\|_2 + \ (\delta t(\mathbf{k}) - \delta t(\mathbf{k})) + v(\mathbf{k}) \tag{4}$$

where $\mathbf{k}$ represents discrete-time $= \mathbf{k} - \delta t$ with δt being the transmission delay of the signal. The term v is the measurement noise, which is modeled as a zero-mean white Gaussian sequence with variance σ^2.

III. OBSERVABILITY ANALYSIS

This section summarizes the analytical observability results derived in (Sabbagh and Kassas, 2023) for receiver localization with a single LEO satellite under two scenarios. The first scenario considers a receiver with *unknown* position states but *known* clock error states. Results from this simple scenario will serve as a stepping stone towards the second scenario, which considers a receiver with *unknown* position states and *unknown* clock error states. In each scenario, the satellite's states are assumed to be known, which is the case whenever (i) a satellite transmits its ephemeris and clock errors (e.g., Orbcomm satellites transmit their states, estimated from onboard GPS receivers (Kassas, 2021)) or (ii) an estimator is employed to estimate the LEO satellite's states (e.g., via a differential navigation framework utilizing a known base receiver (Khalife et al., 2020), via a simultaneous tracking and navigation (STAN) framework (Kassas, 2021)), or via an analytical and/or machine-learning satellite tracking framework (Shen et al., 2019; Khairallah and Kassas, 2021; Haidar-Ahmad et al., 2022)). It is worth noting that instead of estimating the receiver's clock error states, the following analysis readily extends to the case of estimating the *difference* between the receiver's and LEO satellite's clock error states (Khairallah and Kassas, 2022), $\Delta \delta t \triangleq \delta t - \delta t$ and $\Delta \dot{\delta t} \triangleq \dot{\delta t} - \dot{\delta t}$, which could be desirable for stochastic observability considerations (Morales and Kassas, 2019).

The nonlinear pseudorange measurement (4) is linearized at time-step **k** with respect to the unknown receiver states and the corresponding Jacobian matrix is used to build the -step observability matrix. The scenarios are summarized below

- **Scenario 1:** A stationary receiver with *unknown position states* but *known clock error states* makes pseudorange measurements to a LEO satellite with *known states*. The measurement Jacobian is given by $(\mathbf{k}) = \boldsymbol{l}^{\mathsf{T}}$.

- **Scenario 2:** A stationary receiver with *unknown position states and clock error states* makes pseudorange measurements to a LEO satellite with *known states*. The measurement Jacobian is given by $(\mathbf{k}) = \begin{bmatrix} \boldsymbol{l}^{\mathsf{T}} & 1 & 0 \end{bmatrix}$.

Above, $\boldsymbol{l} \in {}^3$ denotes the unit line-of-sight (LOS) vector between the receiver and satellite at time-step **k**, given by

$$\boldsymbol{l} \triangleq \frac{\boldsymbol{r} - \boldsymbol{r}(\mathbf{k})}{\|\boldsymbol{r} - \boldsymbol{r}(\mathbf{k})\|_2}$$

In what follows, the -step observability of the aforementioned scenarios is investigated, and bounds on the determinants of observability matrices therein are derived.

1. *Scenario 1: Pseudorange Measurements with Unknown Receiver Position States but Known Clock Error States*

In this scenario, the only unknown states are the receiver's position, and the 3-step observability matrix is given by

$$\mathcal{O}(\mathbf{k} \ \mathbf{k}+2) = \begin{bmatrix} \boldsymbol{l} & \boldsymbol{l}_{+1} & \boldsymbol{l}_{+2} \end{bmatrix}^{\mathsf{T}} \tag{5}$$

where the transition matrix $\boldsymbol{\Phi} = {}_{3\times3}$ and the measurement Jacobian $(\mathbf{k}) = {}^{\mathsf{T}}$ are used to build $\mathcal{O}(\mathbf{k} \ \mathbf{k}+2)$. Let $\mathcal{O}(\mathbf{k} \ \mathbf{k}+2) \triangleq \mathcal{O}_3$. An expression for $\det(\mathcal{O}_3)$ is derived as a function of the relative geometry between the receiver and the satellite.

Theorem II: Let $\triangleq \cos(\alpha n T)$, $\triangleq \sin(\alpha n T)$, and

$$\beta \triangleq \frac{1}{\|\Delta\boldsymbol{r}(\mathbf{k})\|_2 \, \|\Delta\boldsymbol{r}(\mathbf{k}+1)\|_2 \, \|\Delta\boldsymbol{r}(\mathbf{k}+2)\|_2}$$

where $\Delta\boldsymbol{r}(\mathbf{k}) \triangleq \boldsymbol{r} - \boldsymbol{r}(\mathbf{k})$. The determinant of the 3-step observability matrix in (5) is given by

$$\det(\mathcal{O}_3) = \beta \, (2_{\,1} - {}_2)^{2} \, \sin(\theta) \tag{6}$$

where θ is the angle between the receiver's position vector $\boldsymbol{r}$ and the orbital plane of the LEO satellite.

Proof: The determinant of $\mathcal{O}_3$ is equal to the scalar triple product of its rows which are given by the unit LOS vectors $\boldsymbol{l}$, $\boldsymbol{l}_{+1}$, and $\boldsymbol{l}_{+2}$. Expanding this product in terms of the state variables of the receiver-satellite dynamics will yield the desired result (for details of the proof see (Sabbagh and Kassas, 2023, Theroem II)). ∎

Hereafter, θ is referred to as the *relative orbital inclination angle* between the receiver and the LEO satellite. Ideally, θ is assumed constant for a stationary receiver during the time window through which it is seeing a LEO satellite. In what follows, time-independent bounds on $\det(\mathcal{O}_3)$ are derived.

Corollary I: The determinant of the 3-step observability matrix in (5) can be bounded as follows

$$0 \leq \underline{\Delta}(\theta) \leq \det(\mathcal{O}_3) \leq \overline{\Delta}(\theta)$$

$$\underline{\Delta}(\theta) = \frac{(2 \,_1 - \,_2)^{\,2} \; \sin(\theta)}{(\,^2 + \,^2 + 2 \quad \cos(\theta))^{3\,2}}$$

$$\overline{\Delta}(\theta) = \frac{(2 \,_1 - \,_2)^{\,2} \; \sin(\theta)}{(\,^2 + \,^2 - 2 \quad \cos(\theta))^{3\,2}}$$

where $0 \leq \theta \leq \pi/12$ and $0 \leq \alpha\,k\,T \leq \pi/6$ for all $\mathbf{k} \in$.

Proof: Using the law of cosines, it can be deduced that the coefficient β satisfies $\left(\,^2 + \,^2 + 2 \quad \sin(\theta)\right)^{-3\,2} \leq \beta \leq \left(\,^2 + \,^2 - 2 \quad \sin(\theta)\right)^{-3\,2}$ for all $\mathbf{k} \in$ (for details of the proof see (Sabbagh and Kassas, 2023, Corollary I)). ∎

The inequalities on θ and $\alpha\,k\,T$ are placed with the understanding that a LEO satellite should be visible for a long enough time to provide useful measurements. From the observability analysis of Scenario I, the following can be deduced:

Proposition I: If the receiver is in the orbital plane of the LEO satellite, the system is not -step observable.

Proof: If the receiver is in the orbital plane of the LEO satellite, then $\theta = 0$. This implies that $(\theta) = 0$. As a result, $\det(\mathcal{O}_3) = 0$ and $\mathcal{O}_3$ is rank deficient. In fact, the rows of $\mathcal{O}$, which represent consecutive unit LOS vectors tracing the satellite's orbit, are coplanar lying in the orbital plane of the satellite. As a result, rank$[\mathcal{O}\,] \leq 2$, for all ≥ 2. ∎.

Remark I: The unobservable subspace in the case above is spanned by the normal to the satellite's orbital plane, otherwise known as the satellite's cross direction. This implies that initial receiver position states along this direction are indistinguishable. The impact of this on localization using a single overhead LEO satellite is demonstrated in Section IV.

Proposition II: If the receiver is not in the orbital plane of the LEO satellite, the system is -step observable for ≥ 3.

Proof: If the receiver is not in the orbital plane of the LEO satellite, then $\theta \neq 0$. As a result, $(\theta) \quad (0) \quad 0$, and $\det(\mathcal{O}_3) \neq 0$ with rank$[\mathcal{O}\,] = 3$, for all ≥ 3. In fact, the rows of $\mathcal{O}$, which represent consecutive unit LOS vectors tracing the satellite's orbit, are no longer coplanar. This implies that the corresponding scalar triple product of any three consecutive unit LOS vectors is nonzero within a single orbital period. ∎

2. *Relationship Between the relative orbital inclination θ and the Geometric Diversity of the LOS Vectors*

The above analysis and (6) show that the size of θ normalized by the cube of the receiver-satellite range can measure how close the -step observability matrix is to singularity. In other words,

$$\det(\mathcal{O}_3) \; \propto \; \beta \; \sin(\theta)$$

As a result, a relationship between the singularity of $\mathcal{O}_3$ and the geometric diversity of the unit LOS vectors can be established. Namely, the following observations can be made:

- For small θ, the receiver is near the orbital plane of the satellite so that the LOS vectors are almost *coplanar*.

- For large θ, the receiver is far enough from the satellite so that the LOS vectors are almost *collinear*.

- In both extremes, the LOS vectors have poor geometric diversity.

As a visual aid to illustrate the impact of θ on the determinant of the observability matrix, an exaggerated comparison between the geometric diversity of the LOS vectors created between the LEO satellite and three receivers , , and is shown is shown in Figure 1. These receivers result in three drastically different values of θ, which result in LOS vectors with varying geometric diversity. For example, receiver makes LOS measurements that are relatively closer to each other compared to receiver (large θ), and receiver makes LOS measurements that are coplanar in the orbital plane of the LEO satellite (small θ).

A study on the singularity of $\mathcal{O}_3$ is shown in Figure 2(a), where the values of $\det(\mathcal{O}_3)$ were computed from simulated LOS vectors created between a stationary receiver and a satellite traveling along a circular orbit at an altitude of 521 km (computations were repeated for varying values of $\theta \in [0, \pi/12]$). It is observed that $\det(\mathcal{O}_3)$ drastically diminishes for θ values which are too small or too large, implying that a "favorable" relative orbital inclination region (shown in Figure 2 in yellow) lying in between

the two extremes exists where $\det(\mathcal{O}_3)$ is ideal over the navigation window of the receiver. In summary, for configurations with θ larger than zero, the geometric diversity of the LOS vectors improves up to a certain point, which is a favorable region that optimizes the geometric diversity of the LOS vectors. Upon further increasing θ, the geometric diversity starts to slowly degrade.
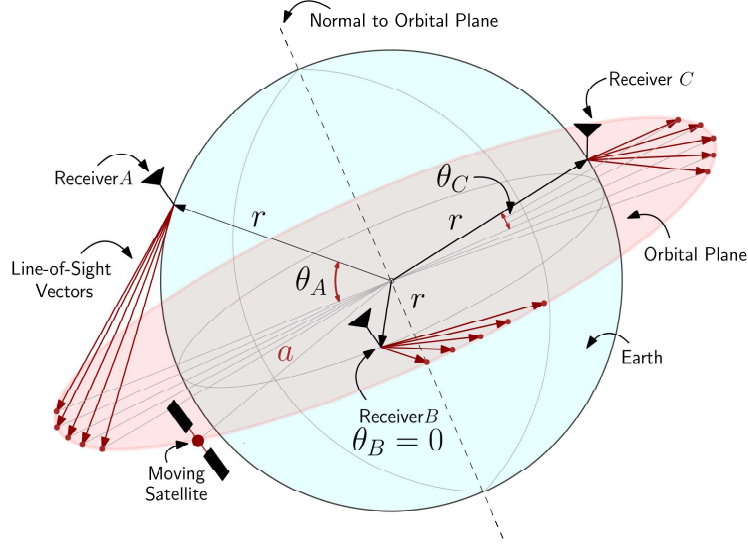
Figure 1: *Comparison between the geometric diversity of the LOS vectors based on the relative orbital inclinations θ_A, θ_B, and θ_C ($\theta_A \gg \theta_C \gg \theta_B$) created between the LEO satellite and receivers A, B, and C, respectively. Receiver A makes LOS measurements that are relatively closer to each other compared to receiver C (large θ), and receiver B makes LOS measurements that are coplanar in the orbital plane of the LEO satellite (small θ).*

3. *Scenario 2: Pseudorange Measurements with Unknown Receiver Position States and Unknown Clock Error States*

In this scenario, the receiver state is unknown, and the 5-step observability matrix is given by

$$\mathcal{O}(\mathbf{k}, \mathbf{k}+4) = \begin{bmatrix} \boldsymbol{l} & \boldsymbol{l}_{+1} & \boldsymbol{l}_{+2} & \boldsymbol{l}_{+3} & \boldsymbol{l}_{+4} \\ 1 & 1 & 1 & 1 & 1 \\ 0 & & 2 & 3 & 4 \end{bmatrix}^{\mathsf{T}} \tag{7}$$

where the transition matrix $\boldsymbol{\Phi} = \ \in\ ^{5\times 5}$ and the measurement Jacobian $(\mathbf{k}) = \begin{bmatrix} \mathsf{T} & 1 & 0 \end{bmatrix} \in\ ^{1\times 5}$ are used to build $\mathcal{O}(\mathbf{k}, \mathbf{k}+4)$. Let $\mathcal{O}(\mathbf{k}, \mathbf{k}+4) \triangleq \mathcal{O}_5$. Next, an expression for $\det(\mathcal{O}_5)$ is derived as a function of the relative geometry between the receiver and the satellite.

Proposition III: Let $\ ,\ ,$ and $\ \in\ $ with $\qquad\quad$, then the following equality holds

$$\boldsymbol{l}\ \cdot (\boldsymbol{l}\ \times \boldsymbol{l}\ ) = \gamma\ \ \ \beta\ \ \ \ ^2\ \ \sin(\theta)$$

where the scalars $\gamma\qquad 0$ and $\beta\qquad 0$ are given by

$$\gamma\qquad \triangleq\ \ \ _-\ +\ \ _-\ -\ \ _-$$

$$\beta\qquad \triangleq\ \frac{1}{\|\Delta\boldsymbol{r}(\mathbf{k}+\ )\|_2\,\|\Delta\boldsymbol{r}(\mathbf{k}+\ )\|_2\,\|\Delta\boldsymbol{r}(\mathbf{k}+\ )\|_2}$$

where $0 \le \theta \le \pi/12$ and $0 \le \alpha\, k\, T \le \pi/6$ for all $\mathbf{k} \in\ $.

Proof: The proof proceeds similarly to that of Theorem II. ∎

Theorem III: The determinant of the 5-step observability matrix in (7) is given by

$$\det(\mathcal{O}_5) =\ \ (\ _1 -\ _2 +\ _3 -\ _4)\ \ ^2\ \ \sin(\theta) \tag{8}$$

where $\aleph_1$, $\aleph_2$, $\aleph_3$, and $\aleph_4$ are scalars given by

$$\aleph_1 = \gamma_{012}\left(\beta_{012} + \beta_{234}\right) + \gamma_{014}\left(\beta_{014} + \beta_{034}\right)$$
$$\aleph_2 = 2\left(\gamma_{013}\,\beta_{013} + \gamma_{024}\,\beta_{024} + \gamma_{134}\,\beta_{134}\right)$$
$$\aleph_3 = 3\,\gamma_{023}\left(\beta_{023} + \beta_{124}\right)$$
$$\aleph_4 = 4\,\gamma_{123}\,\beta_{123}$$

Proof: The determinant of $\mathcal{O}_5$ can be expressed in terms of a product of determinants involving block partitions of $\mathcal{O}_5$ via the Schur complement formula. This yields an alternative expression for $\det(\mathcal{O}_5)$, given by

$$\det(\mathcal{O}_5) = \begin{vmatrix} \boldsymbol{l}^{\mathsf{T}} - 4\,\boldsymbol{l}^{\mathsf{T}}_{+3} + 3\,\boldsymbol{l}^{\mathsf{T}}_{+4} \\ \boldsymbol{l}^{\mathsf{T}}_{+1} - 3\,\boldsymbol{l}^{\mathsf{T}}_{+3} + 2\,\boldsymbol{l}^{\mathsf{T}}_{+4} \\ \boldsymbol{l}^{\mathsf{T}}_{+2} - 2\,\boldsymbol{l}^{\mathsf{T}}_{+3} + \boldsymbol{l}^{\mathsf{T}}_{+4} \end{vmatrix}$$

By expanding the above determinant, the resulting terms can be grouped using Proposition III, resulting in (8). ∎

Time-independent bounds on $\beta_{\mathbf{k}}$ can be derived as in the proof of Corollary I, so that $\aleph^{-3} \leq \beta_{\mathbf{k}} \leq \aleph^{-3}$ for all $\mathbf{k}$, $\aleph$, and $\aleph \in \aleph$. Bounds on $\det(\mathcal{O}_5)$ are presented next.

Corollary II: The determinant of the 5-step observability matrix in (8) can be bounded as follows

$$\aleph(\theta) \leq \det(\mathcal{O}_5) \leq \aleph(\theta)$$
$$\aleph(\theta) = 16\,\aleph^3_1(1-\aleph_1)^2 \aleph\left(\frac{1}{\aleph^3} - \frac{1}{\aleph^3}\right)\sin(\theta)$$
$$\aleph(\theta) = 16\,\aleph^3_1(1-\aleph_1)^2 \aleph\left(\frac{1}{\aleph^3} - \frac{1}{\aleph^3}\right)\sin(\theta)$$

where $0 \leq \theta \leq \pi/12$ and $0 \leq \alpha\,k\,T \leq \pi/6$ for all $\mathbf{k} \in \aleph$.

Proof: The proof proceeds similarly to that of Corollary I. ∎

Based on Theorem III and Corollary II, the following observability results are deduced.

Proposition IV: If the receiver is in the orbital plane of the satellite or along the normal to the orbital plane of the satellite, the system is not $\aleph$-step observable.

Proof: By construction, unobservable directions in Scenario I are inherited into Scenario II where additional receiver states are now unknown. Furthermore, if the receiver is along the normal to the orbital plane of the satellite, the minimum and maximum Euclidean distances between the receiver and the LEO satellite become equal which results in $\aleph(\theta) = \aleph\left(\frac{\pi}{2}\right) = 0$ and $\aleph(\theta) = \aleph\left(\frac{\pi}{2}\right) = 0$, implying that $\det(\mathcal{O}_5) = 0$. In fact, since a constant distance is maintained between the receiver-satellite pair, the stationary receiver can no longer disambiguate between its initial clock bias and the initial range from the satellite, no matter how many pseudorange measurements it makes from that satellite. At best, a one-dimensional unobservable subspace of $\aleph^5$ is maintained, so that $\text{rank}[\mathcal{O}_{\aleph}] \leq 4$, for all $\aleph \geq 4$. ∎

Proposition V: If the receiver is not in the orbital plane of the satellite, nor along the normal to the satellite's orbital plane, the system is $\aleph$-step observable for $\aleph \geq 5$.

Proof: It is enough to show by contradiction that the matrix $\mathcal{O}_5$ in this setting is non-singular (for details of the proof see (Sabbagh and Kassas, 2023, Proposition V)). ∎

4. *Comparison between Scenario I and Scenario II*

The same study on the singularity of $\mathcal{O}_5$ is done and the corresponding observability surface is generated and compared to the previous Scenario. It can be observed that the observability surface in Figure 2(b) is smaller compared to Figure 2(a). This reflects poorer observability conditions and loss of information due to the addition of unknown receiver states to the system. Additionally, while in both scenarios, the determinant of the observability matrix vanishes when the receiver is in the orbital plane, as θ grows past the favorable region, the determinant in Scenario II approaches singularity much faster.
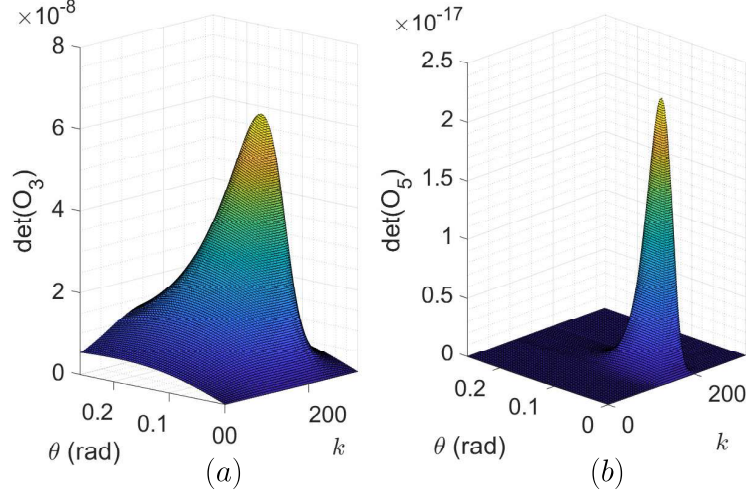
Figure 2: *Values of* $\det(\mathcal{O}_3)$ *(left) and* $\det(\mathcal{O}_5)$ *(right) computed for different values of* θ *in radians at each time-step* k.

Finally, it is important to note that while the unobservable subspaces discussed are of zero measure and assume an ideal setting (perfect knowledge of a circular satellite ephemeris, non-rotating spherical Earth, etc), in a real setting, the satellite's orbit will experience random perturbations such that a receiver localizing itself would not lie along the derived unobservable subspaces. This suggests that theoretically, a receiver with an unknown state can indeed localize itself using pseudorange measurements from a single LEO satellite. Section IV will show the effect of the unobservable direction to receiver localization.

IV. EXPERIMENTAL RESULTS

To demonstrate the conclusions of the observability analysis on receiver localization, an experiment was conducted whereby pseudorange measurements, extracted from carrier phase observables (Khalife et al., 2020, 2022), from one Starlink satellite and one Orbcomm satellite were used to localize a stationary receiver using an EKF for LEO satellite visibility durations of 74 and 317 seconds, respectively. The Starlink and Orbcomm satellites possess average relative orbital inclinations of $\theta = 0\,01457$ rad and $\theta = 0\,00410$ rad, respectively, indicating that the receiver is relatively close to being in their orbital planes during each navigation window. For both satellites, the analysis in Section III shows that the determinant of the corresponding observability

Table 1: Receiver localization error

Satellite	Direction	Initial Error	Final Error
Starlink	Along (m)	-603.94	-67.14
	Cross (m)	-682.25	−768.41
	Radial (m)	-555.90	81.40
	Overall (m)	1,067.35	775.62
Orbcomm	Along (m)	604.47	-51.35
	Cross (m)	-722.25	-689.29
	Radial (m)	-856.47	7.79
	Overall (m)	1,273.30	691.24

matrices is expected to be small enough so that the directions normal to the LEO satellites' orbital planes become nearly unobservable. The objective of the experiment is therefore to demonstrate that receiver localization using near-overhead passing LEO satellites will suffer from poor information in the direction normal to the LEO satellite's orbital plane. This implies that any initial receiver position error in the direction along the normal to the LEO satellite's orbital plane will not reduce in the EKF, due to the observability matrix being nearly singular. For the Starlink satellite, the satellite's states were estimated according to the framework discussed in (Khalife et al., 2022), which estimated the satellite's ephemeris via simplified general perturbation 4 (SGP4) orbit propagator initialized with two-line element (TLE) files. For the Orbcomm satellite, the satellite's states were obtained by decoding the downlink signal, which contains ephemeris and clock errors, estimated via the satellite's onboard GPS receivers (Khalife et al., 2020).

The localization results are shown in Figs. 3 and 4, where the receiver's position estimation errors and the $\pm 3\sigma$-bounds are resolved along the LEO satellite's body frame (along-track, cross-track, and radial directions). Table 1 shows the initial and final receiver position estimation errors in each direction. It can be seen from Figs. 3 and 4 and Table 1 that while the receiver's position error in the along-track and radial directions decreases, there is no improvement in the cross-track direction. This confirms the observability result discussed in Section III, stating that the direction normal to the orbital plane of the satellite is unobservable for a receiver making measurements from incoming overhead satellites.
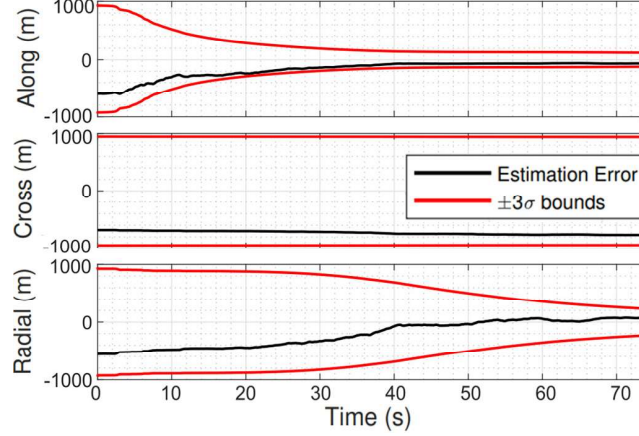
Figure 3: *Receiver position estimation errors resolved along the Starlink satellite body frame (in black) with $\pm 3\sigma$ bounds (in red).*
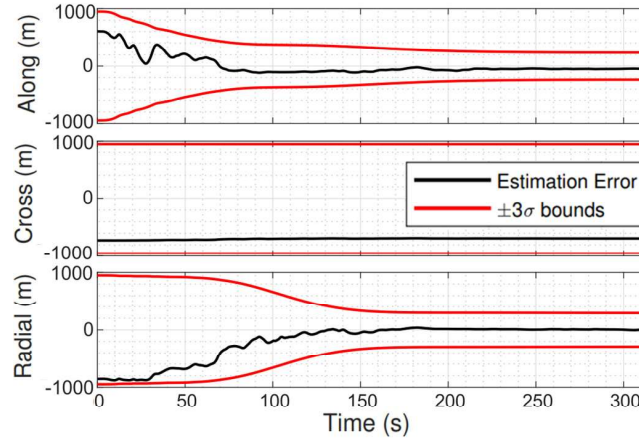

Figure 4: *Receiver position estimation errors resolved along the Orbcomm satellite body frame (in black) with $\pm 3\sigma$ bounds (in red).*

V. OBSERVABILITY-AIDED LEO SATELLITE SELECTION

From a geometric point of view, it may be viable to utilize publicly available TLE files in order to predict LEO satellites that will produce measurements which are most favorable when it comes to the observability of a stationary receiver. Namely, Figure 2 can be utilized for observability-based satellite selection to improve receiver localization based on LEO satellite's SGP4-propagated TLE files. This can be done by mapping the LEO satellite's trajectory with respect to the stationary receiver (which can be guessed *a priori* via information about the satellite's altitudes as well as angles θ of their orbital planes with the receiver) to curves along the observability surfaces (see Figure 5). Then, one may predict and select the satellite which will generate a navigation scenario which is "most" observable by selecting the satellites whose curves are lying in the "favorable" region of the observability surface. Namely, given a set of LEO satellites, one can identify *a priori* the one which will result in the best receiver localization performance, by taking into account the following criteria, which are all features of the observability surfaces shown in Figure 2:

- The visibility duration of the LEO satellite: This can be inferred from the projected length of the satellite's curve on the observability surface, along the time axis.

- The elevation profile of the LEO satellite during this time: This corresponds to the shape of the satellite's curve on the observability surface.

- Satellite altitudes and relative orbital inclinations θ: This corresponds to the position of the satellite's curve on the observability surface, along the θ axis.
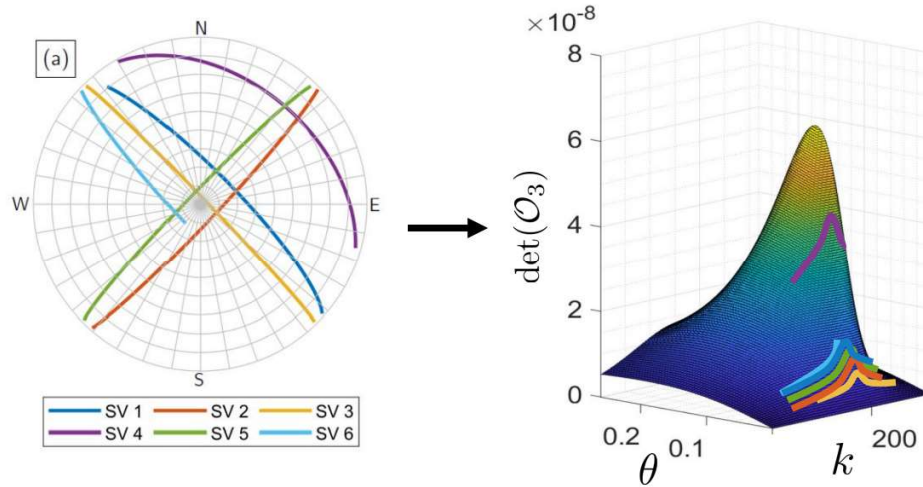
Figure 5: Starlink predicted skyplots

To illustrate the above idea, consider the collection of six Starlink satellites shown in Figure 5. Their propagated TLE files can be used to predict how they will pass above a stationary receiver compared to each other. Knowing *a priori* the average values of their altitudes, θ, and the skyplots shown, it may be possible to map this information directly onto an observability surface, which may then be used to choose the satellite that will provide better measurements. In that case, it is expected that space vehicle (SV) 4 will yield the best localization results, given that it provides measurements for a long enough time and in the "favorable" region from an observability perspective. While the analysis in this paper considered a single LEO satellite, future work could generalize to multiple satellites and develop an observability-aided LEO satellite selection approach that determines the satellites that are expected to provide the best measurements for receiver localization.

ACKNOWLEDGEMENTS

REFERENCES

Bar-Shalom, Y., Li, X., and Kirubarajan, T. (2002). *Estimation with Applications to Tracking and Navigation*. John Wiley & Sons, New York, NY.

Cassel, R., Scherer, D., Wilburne, D., Hirschauer, J., and Burke, J. (2022). Impact of improved oscillator stability on LEO-based satellite navigation. In *Proceedings of ION International Technical Meeting*, pages 893–905.

Elgamoudi, A., Benzerrouk, H., Elango, G., and Landry, R. (2020). Gauss Hermite h∞ filter for UAV tracking using LEO satellites TDOA/FDOA measurement—part I. *IEEE Access*, 8:201428–201440.

Farhangian, F., Benzerrouk, H., and Landry, R. (2021). Opportunistic in-flight INS alignment using LEO satellites and a rotary IMU platform. *Aerospace*, 8(10):280–281.

Farhangian, F. and Landry, R. (2020). Multi-constellation software-defined receiver for Doppler positioning with LEO satellites. *Sensors*, 20(20):5866–5883.

Friedman, A. (2020). *Observability analysis for space situational awareness*. PhD thesis, Purdue University.

Friedman, A. and Frueh, C. (2021). Observability and estimability analysis of geosynchronous objects with angles-only measurements. *The Journal of the Astronautical Sciences*, 68(2):503–534.

Haidar-Ahmad, J., Khairallah, N., and Kassas, Z. (2022). A hybrid analytical-machine learning approach for LEO satellite orbit prediction. In *Proceedings of International Conference on Information Fusion*, pages 1–7.

Hartnett, M. (2022). Performance assessment of navigation using carrier Doppler measurements from multiple LEO constellations. Master's thesis, Air Force Institute of Technology, Wright-Patterson Air Force Base, Ohio, USA.

Huang, C., Qin, H., Zhao, C., and Liang, H. (2022). Phase - time method: Accurate Doppler measurement for Iridium NEXT signals. *IEEE Transactions on Aerospace and Electronic Systems*, pages 1–9.

Huang, G., Mourikis, A., and Roumeliotis, S. (2010). Observability-based rules for designing consistent EKF SLAM estimators. *International Journal of Robotics Research*, 29(5):502–528.

Iannucci, P. and Humphreys, T. (2022). Fused low-Earth-orbit GNSS. *IEEE Transactions on Aerospace and Electronics Systems*. accepted.

Jardak, N. and Jault, Q. (2022). The potential of LEO satellite-based opportunistic navigation for high dynamic applications. *Sensors*, 22(7):2541–2565.

Jiang, M., Qin, H., Zhao, C., and Sun, G. (2022). LEO Doppler-aided GNSS position estimation. *GPS Solutions*, 26(1):1–18.

Judice, A., Venusamy, K., and Livin, J. (2022). Multilayer LEO satellite constellation coverage analysis and its current research directions. In *Proceedings of IEEE International Conference on Distributed Computing and Electrical Circuits and Electronics*, pages 1–5.

Kassas, Z. (2021). Position, navigation, and timing technologies in the 21st century. volume 2, chapter 43: Navigation from low Earth orbit – Part 2: models, implementation, and performance, pages 1381–1412. Wiley-IEEE.

Kassas, Z. and Humphreys, T. (2012). Observability and estimability of collaborative opportunistic navigation with pseudorange measurements. In *Proceedings of ION GNSS Conference*, pages 621–630.

Kassas, Z., Morales, J., and Khalife, J. (2019). New-age satellite-based navigation – STAN: simultaneous tracking and navigation with LEO satellite signals. *Inside GNSS Magazine*, 14(4):56–65.

Kaufman, E., Lovell, T., and Lee, T. (2016). Nonlinear observability for relative orbit determination with angles-only measurements. *The Journal of the Astronautical Sciences*, 63(1):60–80.

Khairallah, N. and Kassas, Z. (2021). Ephemeris closed-loop tracking of LEO satellites with pseudorange and Doppler measurements. In *Proceedings of ION GNSS Conference*, pages 2544–2555.

Khairallah, N. and Kassas, Z. (2022). An interacting multiple model estimator of LEO satellite clocks for improved positioning. In *Proceedings of IEEE Vehicular Technology Conference*, pages 1–5.

Khalife, J., Neinavaie, M., and Kassas, Z. (2020). Navigation with differential carrier phase measurements from megaconstellation LEO satellites. In *Proceedings of IEEE/ION Position, Location, and Navigation Symposium*, pages 1393–1404.

Khalife, J., Neinavaie, M., and Kassas, Z. (2022). The first carrier phase tracking and positioning results with Starlink LEO satellite signals. *IEEE Transactions on Aerospace and Electronic Systems*, 56(2):1487–1491.

Kulu, E. (2021). Satellite constellations–2021 industry survey and trends. In *Proceedings of Annual Small Satellite Conference*, pages 1–20.

Li, M., Xu, T., Guan, M., Gao, F., and Jiang, N. (2022). LEO-constellation-augmented multi-GNSS real-time PPP for rapid re-convergence in harsh environments. *GPS Solutions*, 26(1):1–12.

Liu, S., Gao, Z., Wu, Y., Kwan Ng, D., Gao, X., Wong, K., Chatzinotas, S., and Ottersten, B. (2021). LEO satellite constellations for 5G and beyond: How will they reshape vertical domains? *IEEE Communications Magazine*, 59(7):30–36.

Montenbruck, O. and Gill, E. (2000). *Satellite orbits: models, methods, and applications*. Springer.

Morales, J. and Kassas, Z. (2019). Stochastic observability and uncertainty characterization in simultaneous receiver and transmitter localization. *IEEE Transactions on Aerospace and Electronic Systems*, 55(2):1021–1031.

Nardin, A., Dovis, F., and Fraire, J. (2021). Empowering the tracking performance of LEO-based positioning by means of meta-signals. *IEEE Journal of Radio Frequency Identification*, 5(3):244–253.

Neinavaie, M., Khalife, J., and Kassas, Z. (2022). Acquisition, Doppler tracking, and positioning with Starlink LEO satellites: First results. *IEEE Transactions on Aerospace and Electronic Systems*, 58(3):2606–2610.

Okasha, N., Zekry, A., and Newagy, F. (2022). Hybrid VLC vehicle to vehicle and LEO satellite communication system for highway road coverage. In *Proceedings of International Conference on Computing, Control and Industrial Engineering*, pages 571–583.

Ou, Y. and Zhang, H. (2018). Observability-based Mars autonomous navigation using formation flying spacecraft. *The Journal of Navigation*, 71(1):21–43.

Pike, E., van Graas, F., and Ugazio, S. (2022). Two and three satellite positioning using Doppler and pseudorange. In *Proceedings of International Technical Meeting of The Institute of Navigation*, pages 671–685.

Pinell, C. (2021). Receiver architectures for positioning with low Earth orbit satellite signals. Master's thesis, Lulea University of Technology, School of Electrical Engineering, Sweden.

Prol, F., Ferre, R., Välisuo, Z. S. P., Pinell, C., Lohan, E., Elsanhoury, M., Elmusrati, M., Islam, S., Celikbilek, K., Selvan, K., Yliaho, J., Rutledge, K., Ojala, A., Ferranti, L., andM. Bhuiyan, J. P., Kaasalainen, S., and Kuusniemi, H. (2022). Position, navigation, and timing (PNT) through low earth orbit (LEO) satellites: A survey on current status, challenges, and opportunities. *IEEE Access*, 10:83971–84002.

Psiaki, M. (2021). Navigation using carrier Doppler shift from a LEO constellation: TRANSIT on steroids. *NAVIGATION, Journal of the Institute of Navigation*, 68(3):621–641.

Reid, T., Chan, B., Goel, A., Gunning, K., Manning, B., Martin, J., Neish, A., Perkins, A., and Tarantino, P. (2020). Satellite navigation for the age of autonomy. In *Proceedings of IEEE/ION Position, Location and Navigation Symposium*, pages 342–352.

Reid, T., Walter, T., Enge, P., Lawrence, D., Cobb, H., Gutt, G., O'Conner, M., and Whelan, D. (2021). Position, navigation, and timing technologies in the 21st century. volume 2, chapter 43: Navigation from low Earth orbit – Part 1: Concept, Current Capability, and Future Promise, pages 1359–1379. Wiley-IEEE.

Rugh, W. (1996). *Linear System Theory*. Prentice Hall, Upper Saddle River, NJ, second edition.

Sabbagh, R. and Kassas, Z. (2023). Observability analysis of receiver localization via pseudorange measurements from a single LEO satellite. *IEEE Control Systems Letters*, 7(3):571–576.

Shen, D., Lu, J., Chen, G., Blasch, E., Sheaff, C., Pugh, M., and Pham, K. (2019). Methods of machine learning for space object pattern classification. In *Proceedings of IEEE National Aerospace and Electronics Conference*, pages 565–572.

Sullivan, J., Lovell, T., and D'Amico, S. (2018). Angles-only navigation for autonomous on-orbit space situational awareness applications. In *Proceedings of AAS/AIAA Astrodynamics Specialist Conference*.

Tan, Z., Qin, H., Cong, L., and Zhao, C. (2019). New method for positioning using IRIDIUM satellite signals of opportunity. *IEEE Access*, 7:83412–83423.

Thompson, S., Martin, S., and Bevly, D. (2020). Single differenced Doppler positioning with low Earth orbit signals of opportunity and angle of arrival estimation. In *Proceedings of ION International Technical Meeting*, pages 497–509.

Wang, K. and El-Mowafy, A. (2022). LEO satellite clock analysis and prediction for positioning applications. *Geo-spatial Information Science*, 25(1):14–33.

Wei, Q., Chen, X., and Zhan, Y. (2020). Exploring implicit pilots for precise estimation of LEO satellite downlink Doppler frequency. *IEEE Communications Letters*, 24(10):2270–2274.

Yong, L. and Zhang, A. (2019). Observability analysis and autonomous navigation for two satellites with relative position measurements. *Acta Astronautica*, 163:77–86.

Zhao, C., Qin, H., and Li, Z. (2022). Doppler measurements from multiconstellations in opportunistic navigation. *IEEE Transactions on Instrumentation and Measurement*, 71:1–9.